

# Non-linear screening effects in high energy hadronic interactions

S. Ostapchenko

*Forschungszentrum Karlsruhe, Institut für Kernphysik, 76021 Karlsruhe, Germany*

*D. V. Skobeltsyn Institute of Nuclear Physics, Moscow State University, 119992 Moscow, Russia*

2nd December 2024

## Abstract

Non-linear effects in hadronic interactions are treated by means of enhanced pomeron diagrams, assuming that pomeron-pomeron coupling is dominated by soft partonic processes. It is shown that the approach allows to resolve a seeming inconsistency between realistic parton momentum distributions, measured in deep inelastic scattering experiments, and the energy behavior of total proton-proton cross section. An important feature of the proposed scheme is that the contribution of semi-hard processes to the interaction eikonal contains a significant non-factorizable part. On the other hand, the approach preserves the QCD factorization picture for inclusive high- $p_t$  jet production.

## 1 Introduction

One of the most important issues in high energy physics is the interplay between soft and hard processes in hadronic interactions. The latter involve parton evolution in the region of comparatively high virtualities  $q^2$  and can be treated within the perturbative QCD framework. Despite the smallness of the running coupling  $\alpha_s(q^2)$  involved, corresponding contributions are expected to dominate hadronic interactions at sufficiently high energies, being enhanced by large parton multiplicities and by large logarithmic ratios of parton transverse and longitudinal momenta [1]. On the other hand, very peripheral hadronic collisions are likely to remain governed by non-perturbative soft partonic processes, whose contribution to elastic scattering amplitude thus remains significant even at very high energies. Furthermore, considering production of high transverse momentum particles, one may expect that a significant part of the underlying parton cascades, which mediate the interaction, develops in the non-perturbative low virtuality region [2], apart from the fact that additional soft re-scattering processes may proceed in parallel to the mentioned “semi-hard” ones.

A popular scheme for a combined description of soft and hard processes is the mini-jet approach [3], employed in a number of Monte Carlo generators [4]. There, one treats hadronic collisions within the eikonal framework, considering the interaction eikonal to be the sum of “soft” and “semi-hard” contributions:

$$\chi_{ad}(s, b) = \sigma_{ad}^{\text{soft}}(s) A_{ad}(b) + \sigma_{ad}^{\text{mini-jet}}(s, p_{t,\min}) A_{ad}(b), \quad (1)$$

where the overlap function  $A_{ad}(b)$  is the convolution of electro-magnetic form-factors of hadrons  $a$  and  $d$ ,  $A_{ad}(b) = \int d^2 b' T_a^{\text{e/m}}(b') T_d^{\text{e/m}}(|\vec{b} - \vec{b}'|)$ ,  $\sigma_{ad}^{\text{soft}}(s)$  - a parameterized “soft” parton cross section, and  $\sigma_{ad}^{\text{mini-jet}}(s, p_{t,\min})$  is the inclusive cross section for production of parton jets with transverse momentum bigger than a chosen cutoff  $p_{t,\min}$ , for which the leading logarithmic QCD result is generally used.

Qualitatively similar is the “semi-hard pomeron” scheme [5, 6], where hadronic interactions are treated within the Gribov’s reggeon approach [7, 8] as multiple exchanges of “soft” and “semi-hard” pomerons, the two objects corresponding to soft and semi-hard re-scattering processes.

However, both approaches face a fundamental difficulty when confronted with available experimental data: it appears impossible to accommodate realistic parton momentum distributions, when calculating the mini-jet cross section  $\sigma_{ad}^{\text{mini-jet}}$  in (1), without being in contradiction with moderately slow energy rise of total proton-proton cross section. It seems natural to relate this problem to the contribution of non-linear parton processes, which are missing in the above-discussed eikonal scheme. Indeed, the need for such corrections appears quite evident when considering small  $x$  behavior of parton momentum distribution functions (PDFs) at some finite virtuality scale  $Q^2$ : due to a fast increase of, e.g., gluon PDF  $G(x, Q^2)$  in the  $x \rightarrow 0$  limit parton density in a restricted volume may reach arbitrarily large values [1]. In the QCD framework one describes non-linear parton effects as merging of parton ladders, some typical contributions shown in Fig. 1. In particular, one

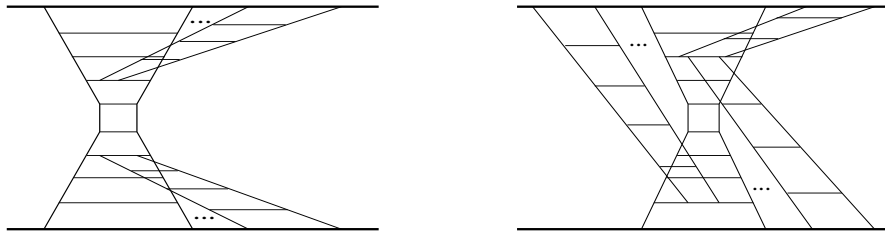


Figure 1: Examples of diagrams giving rise to non-linear parton effects; increasing parton virtualities are indicated as narrowing of the ladders.

may account for such corrections in the perturbative evolution of parton distributions, which leads to the saturation of parton densities [1, 9]. Moving towards smaller and smaller parton momentum fractions  $x$ , one obtains a larger saturation scale  $Q_{\text{sat}}^2(x)$ , with a dynamical parton evolution being only possible in the region of sufficiently high virtualities  $|q|^2 > Q_{\text{sat}}^2(x)$ .

Using the mini-jet approach, one usually suggests some energy dependence for the transverse momentum cutoff  $p_{t,\min}$  for mini-jet production, i.e.  $p_{t,\min} = p_{t,\min}(s)$ , and proceeds further with the usual eikonal expression (1). There, the  $p_t$ -cutoff plays the role of an effective “saturation scale”, for which a variety of empirical parameterizations has been proposed [10]. The underlying idea is to take effectively into account the contributions of diagrams of Fig. 1(left), where non-linear corrections (merging ladders) can be absorbed into parton distributions. Unfortunately, introducing such empirical parameterizations for the  $p_t$ -cutoff, one loses the connection to the perturbative QCD and spoils predictive power of the method; the “saturation scale” is chosen irrespective the actual parton densities, which depend on the parton momenta, on the “centrality” of the interaction, and on the projectile and target mass numbers in case of nuclear collisions. On the other hand, there is no good reason for keeping the simple relation (1) between the interaction eikonal and the mini-jet cross section, when contributions of graphs of Fig. 1(right) are taken into account.

In this paper a phenomenological treatment of non-linear screening corrections is developed in the framework of Gribov’s reggeon approach, describing the latter by means of enhanced (pomeron-pomeron interaction) diagrams [11, 12]. We employ the “semi-hard pomeron” approach, taking into account both soft and semi-hard re-scattering processes. Assuming that pomeron-pomeron coupling is dominated by non-perturbative soft processes and using a phenomenological eikonal parameterization for multi-pomeron vertices, we account for enhanced corrections to hadronic scattering amplitude and to total and diffractive structure functions (SFs)  $F_2, F_2^{D(3)}$ . This allowed us to obtain a consistent description of total and elastic proton-proton cross sections, of the elastic scattering slope, and of the SFs, using a fixed energy-independent virtuality cutoff for semi-hard processes. In particular, we obtained significant corrections to the simple factorized expression (1),

which emerge from enhanced diagrams of the kind of Fig. 1(right), where at least one pomeron (additional parton ladder) is exchanged in parallel to the hardest parton scattering process. On the other hand, due to the Abramovskii-Gribov-Kancheli (AGK) cancellations [13], such diagrams do not contribute significantly to inclusive parton spectra and the usual factorization picture remains applicable for inclusive high  $p_t$  jet production.

The outline of the paper is as follows. Section 2 provides a brief overview of the “semi-hard pomeron” approach. Section 3 is devoted to the treatment of enhanced diagram contributions. Finally, the numerical results obtained are discussed in Section 4.

## 2 Linear scheme

Using Gribov’s reggeon approach [7], a high energy hadron-hadron collision can be described as a multiple scattering process, with elementary re-scatterings being treated phenomenologically as pomeron exchanges, as shown in Fig. 2. Correspondingly, hadron  $a$  - hadron  $d$  elastic scattering

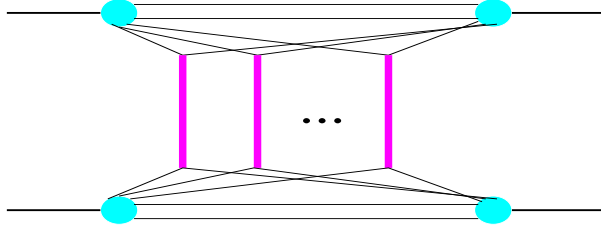


Figure 2: A general multi-pomeron contribution to hadron-hadron scattering amplitude; elementary scattering processes (vertical thick lines) are described as pomeron exchanges<sup>1</sup>.

amplitude can be obtained summing over any number  $n$  of pomeron exchanges<sup>1</sup> [8, 14]:

$$i f_{ad}(s, b) = \sum_{j,k} C_{a(j)} C_{d(k)} \sum_{n=1}^{\infty} \frac{1}{n!} \int \prod_{l=1}^n [dx_l^+ dx_l^- (-\lambda_{a(j)} \lambda_{d(k)} G_{ad}^{\mathbb{P}}(x_l^+ x_l^- s, b))] \times N_a^{(n)}(x_1^+, \dots, x_n^+) N_d^{(n)}(x_1^-, \dots, x_n^-), \quad (2)$$

where  $s$  and  $b$  are c.m. energy squared and impact parameter for the interaction,  $G_{ad}^{\mathbb{P}}(x^+ x^- s, b)$  is the un-integrated pomeron exchange eikonal (for fixed values of pomeron light cone momentum shares  $x^{\pm}$ ), and  $N_a^{(n)}(x_1, \dots, x_n)$  is the light cone momentum distribution of constituent partons - pomeron “ends”.  $C_{a(j)}$  and  $\lambda_{a(j)}$  are correspondingly relative weights and relative strengths of diffractive eigenstates of hadron  $a$  in Good-Walker formalism [15],  $\sum_j C_{a(j)} = 1$ ,  $\sum_j C_{a(j)} \lambda_{a(j)} = 1$ . In particular, two-component picture ( $j = 1, 2$ ) with one “passive” component,  $\lambda_{a(2)} \equiv 0$ , corresponds to the usual quasi-eikonal approach [16], with  $\lambda_{a(1)} \equiv 1/C_{a(1)}$  being the shower enhancement coefficient.

Assuming a factorized form<sup>2</sup> for  $N_a^{(n)}$ , i.e.  $N_a^{(n)}(x_1, \dots, x_n) = \prod_{i=1}^n N_a^{(1)}(x_i)$ , one can simplify (2):

$$f_{ad}(s, b) = i \sum_{j,k} C_{a(j)} C_{d(k)} \left[ 1 - e^{-\lambda_{a(j)} \lambda_{d(k)} \chi_{ad}^{\mathbb{P}}(s, b)} \right] \quad (3)$$

$$\chi_{ad}^{\mathbb{P}}(s, b) = \int dx^+ dx^- G_{ad}^{\mathbb{P}}(x^+ x^- s, b) N_a^{(1)}(x^+) N_d^{(1)}(x^-), \quad (4)$$

<sup>1</sup>In the high energy limit all amplitudes can be considered as pure imaginary.

<sup>2</sup>Here we neglect momentum correlations between multiple re-scattering processes [14].

where the vertex  $N_a^{(1)}(x)$  can be parameterized as  $N_a^{(1)}(x) \sim x^{-\alpha_{\text{part}}}(1-x)^{\alpha_a^{\text{lead}}}$ , with the parameters  $\alpha_{\text{part}} \simeq 0$ ,  $\alpha_p^{\text{lead}} \simeq 1.5$  related to intercepts of secondary reggeon trajectories [16, 17].

This leads to traditional expressions for total and elastic cross sections and for elastic scattering slope:

$$\sigma_{ad}^{\text{tot}}(s) = 2 \text{Im} \int d^2 b f_{ad}(s, b) = 2 \sum_{j,k} C_{a(j)} C_{d(k)} \int d^2 b \left[ 1 - e^{-\lambda_{a(j)} \lambda_{d(k)} \chi_{ad}^{\mathbb{P}}(s, b)} \right] \quad (5)$$

$$\sigma_{ad}^{\text{el}}(s) = \int d^2 b \left[ \sum_{j,k} C_{a(j)} C_{d(k)} \left( 1 - e^{-\lambda_{a(j)} \lambda_{d(k)} \chi_{ad}^{\mathbb{P}}(s, b)} \right) \right]^2 \quad (6)$$

$$B_{ad}^{\text{el}}(s) = \frac{d}{dt} \ln \frac{d\sigma_{ad}^{\text{el}}(s, t)}{dt} \Big|_{t=0} = \frac{1}{\sigma_{ad}^{\text{tot}}(s)} \sum_{j,k} C_{a(j)} C_{d(k)} \int d^2 b b^2 \left[ 1 - e^{-\lambda_{a(j)} \lambda_{d(k)} \chi_{ad}^{\mathbb{P}}(s, b)} \right], \quad (7)$$

where  $d\sigma_{ad}^{\text{el}}(s, t)/dt$  is the differential elastic cross section for momentum transfer squared  $t$ .

In this scheme the pomeron provides an effective description of a microscopic parton cascade, which mediates the interaction between the projectile and the target hadrons. At moderate energies the underlying parton cascade for the pomeron exchange consists mainly of “soft” partons of small virtualities and can be treated in a purely phenomenological way. The corresponding eikonal can be chosen as [8]

$$G_{ad}^{\mathbb{P}_{\text{soft}}}(\hat{s}, b) = \frac{\gamma_0^2 (\hat{s}/s_0)^\Delta}{R_a^2 + R_d^2 + \alpha'_{\mathbb{P}}(0) \ln(\hat{s}/s_0)} \exp \left[ -\frac{b^2}{4(R_a^2 + R_d^2 + \alpha'_{\mathbb{P}}(0) \ln(\hat{s}/s_0))} \right], \quad (8)$$

where  $s_0 \simeq 1 \text{ GeV}^2$  is the hadronic mass scale,  $\Delta = \alpha_{\mathbb{P}}(0) - 1$ ,  $\alpha_{\mathbb{P}}(0)$  and  $\alpha'_{\mathbb{P}}(0)$  are the intercept and the slope of the pomeron Regge trajectory,  $R_a^2$  is the Regge slope of hadron  $a$ , and  $\gamma_0$  stands for pomeron coupling to constituent partons.

At higher energies the underlying parton cascade is more and more populated by quarks and gluons of comparatively high virtualities. Dominant contribution comes here from hard scattering of gluons and sea quarks, which are characterized by small shares  $x_h^\pm$  of parent hadron light cone momenta and are thus preceded by extended soft parton cascades (“soft pre-evolution”), covering long rapidity intervals,  $y_{\text{soft}} \sim \ln 1/x_h^\pm$  [2]. One may apply the phenomenological pomeron treatment for the low ( $|q^2| < Q_0^2$ ) virtuality part of the cascade and describe parton evolution at higher virtualities  $|q^2| > Q_0^2$  using pQCD techniques,  $Q_0^2 \sim 1 \div 2 \text{ GeV}^2$  being a reasonable scale for pQCD being applicable. Thus, a cascade which at least partly develops in the large virtuality region (some  $|q^2| > Q_0^2$ ) can be described as an exchange of a “semi-hard pomeron”, the latter being represented by a piece of QCD ladder sandwiched between two soft pomerons<sup>3</sup> [5, 6], see the 2nd graph in the r.h.s. of Fig. 3. Thus, the “general pomeron” eikonal is the sum of soft and semi-hard ones, as shown in Fig. 3, and we have [6, 17]

$$G_{ad}^{\mathbb{P}}(\hat{s}, b) = G_{ad}^{\mathbb{P}_{\text{soft}}}(\hat{s}, b) + G_{ad}^{\mathbb{P}_{\text{sh}}}(\hat{s}, b) \quad (9)$$

$$G_{ad}^{\mathbb{P}_{\text{sh}}}(\hat{s}, b) = \frac{1}{2} \sum_{I,J=g,q_s} \int d^2 b' \int \frac{dx_h^+}{x_h^+} \frac{dx_h^-}{x_h^-} G_{aI}^{\mathbb{P}_{\text{soft}}} \left( \frac{s_0}{x_h^+}, b' \right) G_{dJ}^{\mathbb{P}_{\text{soft}}} \left( \frac{s_0}{x_h^-}, |\vec{b} - \vec{b}'| \right) \times \sigma_{IJ}^{\text{QCD}}(x_h^+ x_h^- \hat{s}, Q_0^2). \quad (10)$$

Here  $\sigma_{IJ}^{\text{QCD}}(x_h^+ x_h^- \hat{s}, Q_0^2)$  stands for the contribution of parton ladder with the virtuality cutoff  $Q_0^2$ ;  $I, J$  and  $x_h^+, x_h^-$  are types (gluons and sea quarks) and relative light cone momentum fractions of

<sup>3</sup>Similar approaches have been proposed in [2, 18]; in general, a “semi-hard pomeron” may contain an arbitrary number of  $t$ -channel iterations of soft and hard pomerons. The word “pomeron” appears here in quotes as the corresponding amplitude is not the one of a Regge pole.

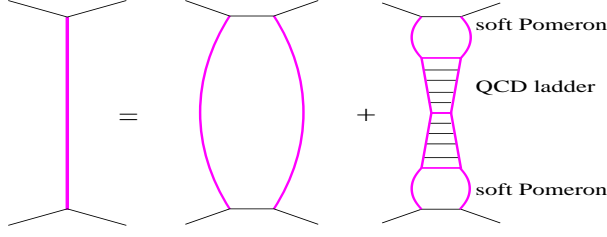


Figure 3: A “general pomeron” (l.h.s.) consists of the soft and semi-hard ones - correspondingly the 1st and the 2nd contributions in the r.h.s.

ladder leg partons:

$$\sigma_{IJ}^{\text{QCD}}(\hat{s}, Q_0^2) = K \sum_{I', J'} \int dz^+ dz^- \int dp_t^2 E_{I \rightarrow I'}^{\text{QCD}}(z^+, Q_0^2, M_F^2) E_{J \rightarrow J'}^{\text{QCD}}(z^-, Q_0^2, M_F^2) \times \frac{d\sigma_{I' J'}^{2 \rightarrow 2}(z^+ z^- \hat{s}, p_t^2)}{dp_t^2} \Theta(M_F^2 - Q_0^2), \quad (11)$$

where  $d\sigma_{I' J'}^{2 \rightarrow 2}/dp_t^2$  is the differential parton-parton cross section,  $p_t$  being the parton transverse momentum in the hard process,  $M_F^2$  - the factorization scale (here  $M_F^2 = p_t^2/4$ ), the factor  $K \simeq 1.5$  takes effectively into account higher order QCD corrections, and  $E_{I \rightarrow I'}^{\text{QCD}}(z, Q_0^2, Q^2)$  describes parton evolution from scale  $Q_0^2$  to  $Q^2$ .

The eikonal  $G_{aI}^{\mathbb{P}_{\text{soft}}}(\hat{s}, b)$ , corresponding to soft pomeron exchange between hadron  $a$  and parton  $I$ , is obtained from (8) replacing one vertex  $\gamma_0$  by a parameterized pomeron-parton vertex  $\gamma_I(z)$ ,  $z = s_0/\hat{s}$ , and neglecting a small slope of pomeron-parton coupling  $R_I^2 \sim 1/Q_0^2$ , which gives

$$G_{aI}^{\mathbb{P}_{\text{soft}}}(\hat{s}, b) = \frac{\gamma_0 \gamma_I(s_0/\hat{s}) (\hat{s}/s_0)^\Delta}{R_a^2 + \alpha'_\mathbb{P}(0) \ln(\hat{s}/s_0)} \exp\left[-\frac{b^2}{4(R_a^2 + \alpha'_\mathbb{P}(0) \ln(\hat{s}/s_0))}\right]. \quad (12)$$

Here we use [6, 17]

$$\gamma_g(z) = r_g (1 - w_{qg}) (1 - z)^{\beta_g} \quad (13)$$

$$\gamma_{q_s}(z) = r_g w_{qg} \int_z^1 dy y^\Delta P_{qg}(y) (1 - z/y)^{\beta_g}, \quad (14)$$

where  $P_{qg}(y) = 3[y^2 + (1 - y)^2]$  is the usual Altarelli-Parisi splitting kernel for three active flavors. By construction, the eikonal  $G_{aI}^{\mathbb{P}_{\text{soft}}}(s_0/x, b)$  describes momentum fraction  $x$  and impact parameter  $b$  distribution of parton  $I$  (gluon or sea quark) in the soft pomeron at virtuality scale  $Q_0^2$ , with the constant  $r_g$  being fixed by parton momentum conservation

$$\int_0^1 dx \int d^2 b [G_{ag}^{\mathbb{P}_{\text{soft}}}(s_0/x, b) + G_{aq_s}^{\mathbb{P}_{\text{soft}}}(s_0/x, b)] = 1. \quad (15)$$

Convoluting  $G_{aI}^{\mathbb{P}_{\text{soft}}}$  with the constituent parton distribution  $N_a^{(1)}(x)$ , one obtains momentum and impact parameter distribution of parton  $I$  in hadron  $a$  at virtuality scale  $Q_0^2$ :

$$x \tilde{f}_{I/a}(x, b, Q_0^2) = \int_x^1 dx' N_a^{(1)}(x') G_{aI}^{\mathbb{P}_{\text{soft}}}\left(\frac{s_0 x'}{x}, b\right). \quad (16)$$

In addition to  $\chi_{ad}^{\mathbb{P}}(s, b)$ , defined by (4), (8–10), one may include contributions of valence quark hard interactions with each other or with sea quarks and gluons<sup>4</sup>  $\chi_{ad}^{\text{val-val}}$ ,  $\chi_{ad}^{\text{val-sea}}$ ,  $\chi_{ad}^{\text{sea-val}}$  [6, 17].

<sup>4</sup>For brevity, in the following these contributions will not be discussed explicitly.

In case of valence quarks one can neglect the “soft pre-evolution” and use for their momentum and impact parameter distribution at scale  $Q_0^2$

$$\tilde{f}_{q_v/a}(x, b, Q_0^2) = \frac{q_v(x, Q_0^2)}{4\pi R_a^2} \exp\left(-\frac{b^2}{4R_a^2}\right), \quad (17)$$

with  $q_v(x, Q_0^2)$  being a parameterized input (here GRV94 [19]).

Correspondingly, the complete hadron-hadron interaction eikonal can be written as [6, 17]

$$\begin{aligned} \chi_{ad}(s, b) &= \chi_{ad}^{\mathbb{P}}(s, b) + \chi_{ad}^{\text{val-val}}(s, b) + \chi_{ad}^{\text{val-sea}}(s, b) + \chi_{ad}^{\text{sea-val}}(s, b) \\ &= \chi_{ad}^{\mathbb{P}_{\text{soft}}}(s, b) + \frac{K}{2} \sum_{I,J} \int dx^+ dx^- \int dp_t^2 \int d^2 b' \tilde{f}_{I/a}(x^+, b', M_F^2) \tilde{f}_{J/d}(x^-, |\vec{b} - \vec{b}'|, M_F^2) \\ &\quad \times \frac{d\sigma_{IJ}^{2 \rightarrow 2}(x^+ x^- s, p_t^2)}{dp_t^2} \Theta(M_F^2 - Q_0^2), \end{aligned} \quad (18)$$

where  $\chi_{ad}^{\mathbb{P}_{\text{soft}}}(s, b) = \int dx^+ dx^- G_{ad}^{\mathbb{P}_{\text{soft}}}(x^+ x^- s, b) N_a^{(1)}(x^+) N_d^{(1)}(x^-)$  and parton momentum and impact parameter distributions  $f_{I/a}(x, b, Q^2)$  at arbitrary scale  $Q^2$  are obtained evolving the input ones (16-17) from  $Q_0^2$  to  $Q^2$ :

$$\tilde{f}_{I/a}(x, b, Q^2) = \sum_{J=g, q_s, q_v} \int_x^1 \frac{dz}{z} E_{J \rightarrow I}^{\text{QCD}}(z, Q_0^2, Q^2) \tilde{f}_{J/a}(x/z, b, Q_0^2). \quad (19)$$

It is noteworthy that the eikonal (18) is similar to the usual ansatz (1) of the mini-jet approach, apart from the fact that in the latter case one assumed a factorized momentum and impact parameter dependence of parton distributions, i.e.

$$\tilde{f}_{I/a}^{\text{mini-jet}}(x, b, Q^2) = f_{I/a}(x, Q^2) T_a^{\text{e/m}}(b). \quad (20)$$

In the above-described approach parton distributions at arbitrary scale  $Q^2$  are obtained from a convolution of “soft” and “hard” parton evolution, the former being described by the soft pomeron asymptotics. As a consequence, partons of smaller virtualities result from a longer “soft” evolution and are distributed over a larger transverse area.

### 3 Non-linear screening corrections

The above-described picture appears to be incomplete in the “dense” regime, i.e. in the limit of high energies and small impact parameters for the interaction. There, a large number of elementary scattering processes occurs and corresponding underlying parton cascades overlap and interact with each other, giving rise to significant non-linear effects. Here we are going to treat non-linear screening effects in the framework of Gribov’s reggeon scheme [7, 8] by means of enhanced pomeron diagrams, which involve pomeron-pomeron interactions [11]. Concerning multi-pomeron vertices, we assume that they are characterized by small slope  $R_{\mathbb{P}}^2$  (neglected in the following) and by eikonal structure, i.e. for the vertex which describes the transition of  $m$  into  $n$  pomerons we use  $g_{mn} = r_{3\mathbb{P}} \gamma_{\mathbb{P}}^{m+n-3} / (4\pi m! n!)$ , with  $r_{3\mathbb{P}}$  being the triple-pomeron coupling. Doing a replacement  $r_{3\mathbb{P}} = 4\pi G \gamma_{\mathbb{P}}^3$  and neglecting momentum spread of pomeron “ends” in the vertices, for a pomeron exchanged between two vertices, separated from each other by rapidity  $y$  and impact parameter  $b$ , we use the eikonal  $G_{\mathbb{P}\mathbb{P}}^{\mathbb{P}}(y, b)$ , being the sum of corresponding soft and semi-hard contributions  $G_{\mathbb{P}\mathbb{P}}^{\mathbb{P}_{\text{soft}}}(y, b)$ ,  $G_{\mathbb{P}\mathbb{P}}^{\mathbb{P}_{\text{sh}}}(y, b)$ . The latter are obtained from  $G_{ad}^{\mathbb{P}_{\text{soft}}}(s_0 e^y, b)$ ,  $G_{ad}^{\mathbb{P}_{\text{sh}}}(s_0 e^y, b)$ , defined in (8), (10-12), replacing the vertex factors  $\gamma_a$ ,  $\gamma_d$  by  $\gamma_{\mathbb{P}}$  and the slopes  $R_a^2$ ,  $R_d^2$  by  $R_{\mathbb{P}}^2 \sim 0$ :

$$G_{\mathbb{P}\mathbb{P}}^{\mathbb{P}}(y, b) = G_{\mathbb{P}\mathbb{P}}^{\mathbb{P}_{\text{soft}}}(y, b) + G_{\mathbb{P}\mathbb{P}}^{\mathbb{P}_{\text{sh}}}(y, b) \quad (21)$$

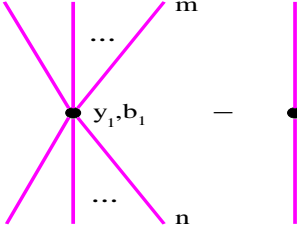


Figure 4: Lowest order enhanced graphs; pomeron connections to the projectile and target hadrons not shown explicitly.

$$G_{\mathbb{P}\mathbb{P}}^{\mathbb{P}_{\text{soft}}}(y, b) = \frac{\gamma_{\mathbb{P}}^2 e^{\Delta y}}{\alpha'_{\mathbb{P}}(0) y} \exp\left[-\frac{b^2}{4\alpha'_{\mathbb{P}}(0) y}\right] \quad (22)$$

$$G_{\mathbb{P}\mathbb{P}}^{\mathbb{P}_{\text{sh}}}(y, b) = \frac{1}{2} \sum_{I,J} \int d^2 b' \int dy^+ dy^- G_{\mathbb{P}I}^{\mathbb{P}_{\text{soft}}}(y^+, b') G_{\mathbb{P}J}^{\mathbb{P}_{\text{soft}}}(y^-, |\vec{b} - \vec{b}'|) \sigma_{IJ}^{\text{QCD}}(s_0 e^{y-y^+-y^-}, Q_0^2) \quad (23)$$

$$G_{\mathbb{P}I}^{\mathbb{P}_{\text{soft}}}(y, b) = \frac{\gamma_{\mathbb{P}} \gamma_I(e^{-y}) e^{\Delta y}}{\alpha'_{\mathbb{P}}(0) y} \exp\left[-\frac{b^2}{4\alpha'_{\mathbb{P}}(0) y}\right]. \quad (24)$$

Similarly, for a pomeron exchanged between hadron  $a$  and a multi-pomeron vertex we use the eikonal  $\chi_{a\mathbb{P}}^{\mathbb{P}}(y, b)$ , defined as

$$\chi_{a\mathbb{P}}^{\mathbb{P}}(y, b) = \int dx N_a^{(1)}(x) \left[ G_{a\mathbb{P}}^{\mathbb{P}_{\text{soft}}}(y - \ln \frac{1}{x}, b) + G_{a\mathbb{P}}^{\mathbb{P}_{\text{sh}}}(y - \ln \frac{1}{x}, b) \right] \quad (25)$$

$$G_{a\mathbb{P}}^{\mathbb{P}_{\text{soft}}}(y, b) = \frac{\gamma_0 \gamma_{\mathbb{P}} e^{\Delta y}}{R_a^2 + \alpha'_{\mathbb{P}}(0) y} \exp\left[-\frac{b^2}{4(R_a^2 + \alpha'_{\mathbb{P}}(0) y)}\right] \quad (26)$$

$$G_{a\mathbb{P}}^{\mathbb{P}_{\text{sh}}}(y, b) = \frac{1}{2} \sum_{I,J} \int d^2 b' \int dy^+ dy^- G_{aI}^{\mathbb{P}_{\text{soft}}}(y^+, b') G_{\mathbb{P}J}^{\mathbb{P}_{\text{soft}}}(y^-, |\vec{b} - \vec{b}'|) \sigma_{IJ}^{\text{QCD}}(s_0 e^{y-y^+-y^-}, Q_0^2). \quad (27)$$

As an example, the contribution of enhanced diagrams with only one multi-pomeron vertex, which are coupled to diffractive eigenstates  $j$  and  $k$  of hadrons  $a$  and  $d$ , can be obtained using standard reggeon calculus techniques [7, 8, 11]: summing over  $m \geq 1$  pomerons exchanged between the vertex and the projectile hadron,  $n \geq 1$  pomeron exchanges between the vertex and the target, subtracting the term with  $m = n = 1$  (pomeron self-coupling), and integrating over rapidity  $y_1 < Y = \ln \frac{s}{s_0}$  and impact parameter  $\vec{b}_1$  of the vertex, as shown in Fig. 4:

$$\begin{aligned} \chi_{ad(jk)}^{\mathbb{P}\mathbb{P}\mathbb{P}(1)}(s, b) &= \frac{G}{\lambda_{a(j)} \lambda_{d(k)}} \sum_{m,n \geq 1; m+n \geq 3} \int_0^Y dy_1 \int d^2 b_1 \frac{[-\lambda_{a(j)} \chi_{a\mathbb{P}}^{\mathbb{P}}(Y - y_1, |\vec{b} - \vec{b}_1|)]^m}{m!} \\ &\times \frac{[-\lambda_{d(k)} \chi_{d\mathbb{P}}^{\mathbb{P}}(y_1, b_1)]^n}{n!} = G \int_0^Y dy_1 \int d^2 b_1 \left\{ \left( 1 - e^{-\lambda_{a(j)} \chi_{a\mathbb{P}}^{\mathbb{P}}(Y - y_1, |\vec{b} - \vec{b}_1|)} \right) \right. \\ &\times \left. \left( 1 - e^{-\lambda_{d(k)} \chi_{d\mathbb{P}}^{\mathbb{P}}(y_1, b_1)} \right) - \lambda_{a(j)} \lambda_{d(k)} \chi_{a\mathbb{P}}^{\mathbb{P}}(Y - y_1, |\vec{b} - \vec{b}_1|) \chi_{d\mathbb{P}}^{\mathbb{P}}(y_1, b_1) \right\}. \end{aligned} \quad (28)$$

Here our key assumption is that pomeron-pomeron coupling proceeds via partonic processes at comparatively low virtualities,  $|q^2| < Q_0^2$ , with  $Q_0$  being a fixed energy-independent parameter [17, 20]. In that case multi-pomeron vertexes involve only interactions between soft pomerons or between the “soft ends” of semi-hard pomerons, as shown in Fig. 5; direct coupling between parton ladders in the region of high virtualities  $|q^2| > Q_0^2$  is neglected.

As shown in [12], the contribution of dominant enhanced diagrams can be represented by the graphs of Fig. 6. With our present conventions the corresponding eikonal contribution can be

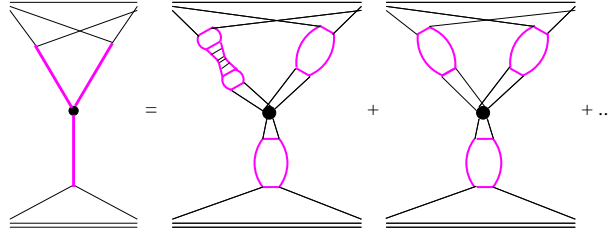


Figure 5: Contributions to the triple-pomeron vertex from interactions between soft and semi-hard pomerons.

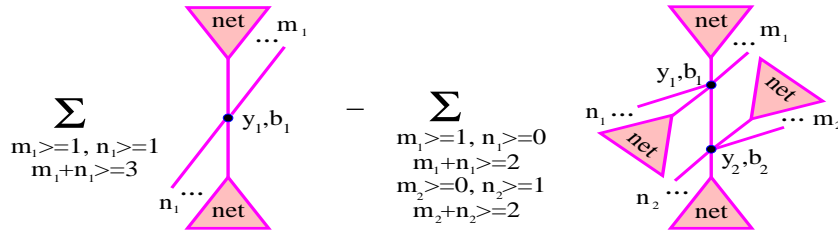


Figure 6: Complete set of dominant enhanced diagrams;  $y_i$ ,  $\vec{b}_i$  ( $i = 1, 2$ ) denote rapidity and impact parameter positions of multi-pomeron vertices,  $i$ -th vertex couples together  $m_i$  projectile and  $n_i$  target “net fans”.

written as<sup>5</sup>

$$\begin{aligned} \chi_{ad(jk)}^{\text{enh}}(s, b) = & \frac{G}{\lambda_{a(j)} \lambda_{d(k)}} \int_0^Y dy_1 \int d^2 b_1 \left\{ \left[ \left( 1 - e^{-\lambda_{a(j)} \chi_{a(j)|d(k)}^{\text{net}}(Y - y_1, \vec{b} - \vec{b}_1 | Y, \vec{b})} \right) \right. \right. \\ & \times \left( 1 - e^{-\lambda_{d(k)} \chi_{d(k)|a(j)}^{\text{net}}(y_1, \vec{b}_1 | Y, \vec{b})} \right) - \lambda_{a(j)} \lambda_{d(k)} \chi_{a(j)|d(k)}^{\text{net}}(Y - y_1, \vec{b} - \vec{b}_1 | Y, \vec{b}) \chi_{d(k)|a(j)}^{\text{net}}(y_1, \vec{b}_1 | Y, \vec{b}) \left. \left. \right] \right. \\ & - G \int_0^{y_1} dy_2 \int d^2 b_2 G_{\mathbb{P}}^{\mathbb{P}}(y_1 - y_2, |\vec{b}_1 - \vec{b}_2|) \left[ \left( 1 - e^{-\lambda_{a(j)} \chi_{a(j)|d(k)}^{\text{net}}(Y - y_1, \vec{b} - \vec{b}_1 | Y, \vec{b})} \right) \right. \\ & \times e^{-\lambda_{d(k)} \chi_{d(k)|a(j)}^{\text{net}}(y_1, \vec{b}_1 | Y, \vec{b})} - \lambda_{a(j)} \chi_{a(j)|d(k)}^{\text{net}}(Y - y_1, \vec{b} - \vec{b}_1 | Y, \vec{b}) \left. \left. \right] \right. \\ & \times \left[ \left( 1 - e^{-\lambda_{d(k)} \chi_{d(k)|a(j)}^{\text{net}}(y_2, \vec{b}_2 | Y, \vec{b})} \right) e^{-\lambda_{a(j)} \chi_{a(j)|d(k)}^{\text{net}}(Y - y_2, \vec{b} - \vec{b}_2 | Y, \vec{b})} - \lambda_{d(k)} \chi_{d(k)|a(j)}^{\text{net}}(y_2, \vec{b}_2 | Y, \vec{b}) \right] \left. \right\}. \end{aligned} \quad (29)$$

Here  $\chi_{a(j)|d(k)}^{\text{net}}(y, \vec{b}_1 | Y, \vec{b})$  stands for the contribution of “net fan” graphs, which correspond to arbitrary “nets” of pomerons, exchanged between hadrons  $a$  and  $d$  (represented by their diffractive components  $j, k$ ), with one pomeron vertex in the “handle” of the “fan” being fixed;  $y, b_1$  are rapidity and impact parameter distances between hadron  $a$  and this vertex. The “net fan” contribution  $\chi_{a(j)|d(k)}^{\text{net}}$  is defined via the recursive equation of Fig. 7 [12]:

$$\begin{aligned} \chi_{a(j)|d(k)}^{\text{net}}(y, \vec{b}_1 | Y, \vec{b}) = & \chi_{a\mathbb{P}}^{\mathbb{P}}(y, b_1) + \frac{G}{\lambda_{a(j)}} \int_0^y dy' \int d^2 b' G_{\mathbb{P}}^{\mathbb{P}}(y - y', |\vec{b}_1 - \vec{b}'|) \\ & \times \left[ \left( 1 - e^{-\lambda_{a(j)} \chi_{a(j)|d(k)}^{\text{net}}(y', \vec{b}' | Y, \vec{b})} \right) e^{-\lambda_{d(k)} \chi_{d(k)|a(j)}^{\text{net}}(Y - y', \vec{b} - \vec{b}' | Y, \vec{b})} - \lambda_{a(j)} \chi_{a(j)|d(k)}^{\text{net}}(y', \vec{b}' | Y, \vec{b}) \right]. \end{aligned} \quad (30)$$

Thus, one can calculate total and elastic cross sections and elastic scattering slope for hadron-hadron scattering, with non-linear screening corrections taken into account, using usual expressions (5-7), with the pomeron eikonal  $\chi_{ad}^{\mathbb{P}}$  being replaced by the sum of  $\chi_{ad}^{\mathbb{P}}$  and  $\chi_{ad(jk)}^{\text{enh}}$ :

$$\chi_{ad(jk)}^{\text{tot}}(s, b) = \chi_{ad}^{\mathbb{P}}(s, b) + \chi_{ad(jk)}^{\text{enh}}(s, b). \quad (31)$$

<sup>5</sup>The expression for  $\chi_{ad}^{\text{enh}}(s, b)$  in [12] corresponds to the quasi-eikonal approach and to the  $\pi$ -meson dominance of multi-pomeron vertices.

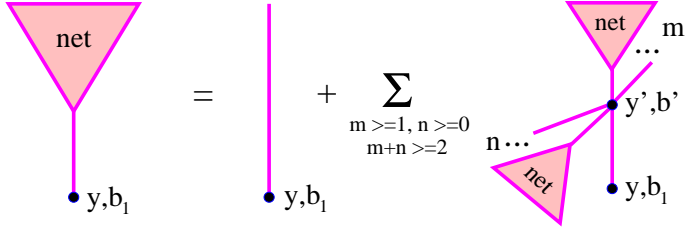


Figure 7: Recursive equation for the projectile “net fan” contribution  $\chi_{a(j)|d(k)}^{\text{net}}(y, \vec{b}_1|Y, \vec{b})$ ;  $y, b_1$  are rapidity and impact parameter distances between hadron  $a$  and the vertex in the “handle” of the “fan”. The vertex  $(y', b')$  couples together  $m$  projectile and  $n$  target “net fans”.

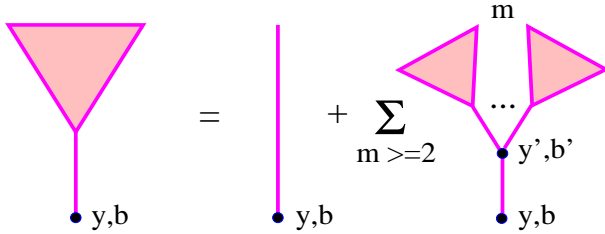


Figure 8: Recursive equation for the projectile “fan” contribution  $\chi_{a(j)}^{\text{fan}}(y, b)$ ;  $y$  and  $b$  are rapidity and impact parameter distances between hadron  $a$  and the vertex in the “handle” of the “fan”. The vertex  $(y', b')$  couples together  $m$  projectile “fans”.

Let us also derive screening corrections to parton (sea quark and gluon) momentum and impact parameter distributions  $\tilde{f}_{I/a}(x, b, Q^2)$ , which come from diagrams of “fan” type [1]. In our scheme the general “fan” contribution can be obtained solving iteratively the recursive equation of Fig. 8, which is a particular case of more general “net fan” equation of Fig. 7, when all intermediate vertices are connected to hadron  $a$  only (i.e.  $n \equiv 0$  in Fig. 7):

$$\begin{aligned} \chi_{a(j)}^{\text{fan}}(y, b) &= \chi_{a\mathbb{P}}^{\mathbb{P}}(y, b) + \frac{G}{\lambda_{a(j)}} \int_0^y dy' \int d^2 b' G_{\mathbb{P}\mathbb{P}}^{\mathbb{P}}(y - y', |\vec{b} - \vec{b}'|) \\ &\quad \times \left[ 1 - e^{-\lambda_{a(j)} \chi_{a(j)}^{\text{fan}}(y', b')} - \lambda_{a(j)} \chi_{a(j)}^{\text{fan}}(y', b') \right]. \end{aligned} \quad (32)$$

Then, parton distributions  $x \tilde{f}_{I/a}^{\text{scr}}(x, b, Q_0^2)$  ( $I = g, q_s$ ) are defined by diagrams of Fig. 8 with  $y = -\ln x$  and with the down-most vertices being replaced by the pomeron-parton coupling, which amounts to replace the eikonal  $\chi_{a\mathbb{P}}^{\mathbb{P}}(y, b)$ ,  $G_{\mathbb{P}\mathbb{P}}^{\mathbb{P}}(y - y', |\vec{b} - \vec{b}'|)$  in (32) by  $x \tilde{f}_{I/a}(x, b, Q_0^2)$ ,  $G_{\mathbb{P}I}^{\mathbb{P}\text{soft}}(-\ln x - y', |\vec{b} - \vec{b}'|)$  correspondingly, the latter being defined in (16), (24). Thus, averaging over diffractive eigenstates of hadron  $a$  with the corresponding weights  $C_{a(j)} \lambda_{a(j)}$ , we obtain

$$\begin{aligned} x \tilde{f}_{I/a}^{\text{scr}}(x, b, Q_0^2) &= x \tilde{f}_{I/a}(x, b, Q_0^2) + G \sum_j C_{a(j)} \int_0^{-\ln x} dy' \int d^2 b' G_{\mathbb{P}I}^{\mathbb{P}\text{soft}}(-\ln x - y', |\vec{b} - \vec{b}'|) \\ &\quad \times \left[ 1 - e^{-\lambda_{a(j)} \chi_{a(j)}^{\text{fan}}(y', b')} - \lambda_{a(j)} \chi_{a(j)}^{\text{fan}}(y', b') \right]. \end{aligned} \quad (33)$$

Parton distributions  $\tilde{f}_{I/a}(x, b, Q^2)$  at arbitrary scale  $Q^2$  are obtained substituting  $\tilde{f}_{J/a}(x, b, Q_0^2)$  in (19) by  $\tilde{f}_{J/a}^{\text{scr}}(x, b, Q_0^2)$  as the initial conditions for sea quarks and gluons.

Let us finally obtain diffractive parton distributions, which are relevant for diffractive deep inelastic scattering reactions, when a large rapidity gap, not covered by secondary particle production, appears in the process. First, we have to obtain the contribution of unitarity cuts of

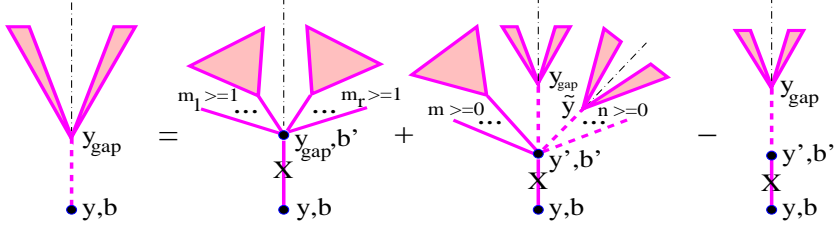


Figure 9: Recursive equation for the diffractive “fan” contribution  $\chi_{a(j)}^{\text{diffr}}(y, b, y_{\text{gap}})$ ;  $y, b$  are rapidity and impact parameter distances between hadron  $a$  and the vertex in the “handle” of the “fan”,  $y_{\text{gap}}$  is the size of the rapidity gap. Dot-dashed lines indicate the position of the cut plane; cut pomerons are marked by crosses.

the “fan” diagrams of Fig. 8, which lead to a rapidity gap of size  $y_{\text{gap}}$  between hadron  $a$  and the nearest particle produced after the gap. Introducing a generic symbol for the diffractive contribution  $\chi_{a(j)}^{\text{diffr}}(y, b, y_{\text{gap}})$  as a “fork” with broken “handle”, applying AGK cutting rules [13] to the 2nd graph in the r.h.s. of Fig. 8, and collecting cut diagrams of diffractive type, we obtain for  $\chi_{a(j)}^{\text{diffr}}$  the recursive equation shown in Fig. 9:

$$\begin{aligned} \chi_{a(j)}^{\text{diffr}}(y, b, y_{\text{gap}}) = & \frac{G}{\lambda_{a(j)}} \int d^2 b' \left\{ \frac{1}{2} \left[ 1 - e^{-\lambda_{a(j)} \chi_{a(j)}^{\text{fan}}(y_{\text{gap}}, b')} \right]^2 G_{\mathbb{P}\mathbb{P}}^{\mathbb{P}}(y - y_{\text{gap}}, |\vec{b} - \vec{b}'|) \right. \\ & + \int_{y_{\text{gap}}}^y dy' \lambda_{a(j)} \chi_{a(j)}^{\text{diffr}}(y', b', y_{\text{gap}}) G_{\mathbb{P}\mathbb{P}}^{\mathbb{P}}(y - y', |\vec{b} - \vec{b}'|) \\ & \left. \times \left[ \exp \left( -2\lambda_{a(j)} \chi_{a(j)}^{\text{fan}}(y', b') + \int_{y_{\text{gap}}}^{y'} d\tilde{y} 2\lambda_{a(j)} \chi_{a(j)}^{\text{diffr}}(y', b', \tilde{y}) \right) - 1 \right] \right\}. \end{aligned} \quad (34)$$

The first graph in the r.h.s. of Fig. 9 is obtained when the cut plane passes between the “fans” connected to the vertex  $(y', b')$  in Fig. 8 (in which case we have  $y' = y_{\text{gap}}$ ), with any number but at least one “fan” remained on either side of the cut. Correspondingly the 2nd diagram appears when the cut goes through at least one of the “fans”, producing a rapidity gap of size  $y_{\text{gap}}$  inside. Then, the vertex  $(y', b')$  is coupled to the diffractive “fan”  $\chi_{a(j)}^{\text{diffr}}(y', b', y_{\text{gap}})$  and to any number  $m \geq 0$  of uncut “fans”, each of which may be positioned on either side of the cut. Also, any number  $n \geq 0$  of additional diffractively cut “fans” may be connected to this vertex, provided all of them produce rapidity gaps larger than  $y_{\text{gap}}$ :  $\tilde{y}_i \geq y_{\text{gap}}$ ,  $i = 1, \dots, n$ . Finally, the last graph in the r.h.s. of Fig. 9 is to subtract the pomeron self-coupling contribution ( $m = n = 0$ ).

In turn, diffractive PDFs  $x x_{\mathbb{P}} f_{I/a}^{\text{diffr}}(x, x_{\mathbb{P}}, Q_0^2)$  are obtained from diagrams of Fig. 9 with  $y = -\ln x$ ,  $y_{\text{gap}} = -\ln x_{\mathbb{P}}$ , replacing the down-most vertex by pomeron-parton coupling (replacing the eikonal  $G_{\mathbb{P}\mathbb{P}}^{\mathbb{P}}$  in (34) by  $G_{\mathbb{P}I}^{\mathbb{P}\text{soft}}$ ), averaging over diffractive eigenstates of hadron  $a$ , and integrating over impact parameter  $b$ :

$$\begin{aligned} x x_{\mathbb{P}} f_{I/a}^{\text{diffr}}(x, x_{\mathbb{P}}, Q_0^2) = & 4\pi G \gamma_{\mathbb{P}} x^{-\Delta} \sum_j C_{a(j)} \int d^2 b' \left\{ \frac{1}{2} \gamma_I \left( \frac{x}{x_{\mathbb{P}}} \right) x_{\mathbb{P}}^{\Delta} \left[ 1 - e^{-\lambda_{a(j)} \chi_{a(j)}^{\text{fan}}(-\ln x_{\mathbb{P}}, b')} \right]^2 \right. \\ & + \int_{-\ln x_{\mathbb{P}}}^{-\ln x} dy' \gamma_I \left( x e^{y'} \right) e^{-\Delta y'} \lambda_{a(j)} \chi_{a(j)}^{\text{diffr}}(y', b', -\ln x_{\mathbb{P}}) \\ & \left. \times \left[ \exp \left( -2\lambda_{a(j)} \chi_{a(j)}^{\text{fan}}(y', b') + \int_{-\ln x_{\mathbb{P}}}^{y'} d\tilde{y} 2\lambda_{a(j)} \chi_{a(j)}^{\text{diffr}}(y', b', \tilde{y}) \right) - 1 \right] \right\}. \end{aligned} \quad (35)$$

At arbitrary scale  $Q^2$  we thus have

$$f_{I/a}^{\text{diffr}}(x, x_{\mathbb{P}}, Q^2) = \sum_{J=g, q_s} \int_{x/x_{\mathbb{P}}}^1 \frac{dz}{z} E_{J \rightarrow I}^{\text{QCD}}(z, Q_0^2, Q^2) f_{J/a}^{\text{diffr}}(x/z, x_{\mathbb{P}}, Q_0^2). \quad (36)$$

It is noteworthy that (35-36) are only applicable for large mass diffraction ( $\beta = x/x_{\mathbb{P}} \ll 1$ ), as at moderate  $\beta$  dominant contribution comes from the so-called  $q\bar{q}$  diffraction component [21], which is neglected here.

## 4 Results and discussion

The obtained formulas have been applied to calculate total and elastic proton-proton cross sections and elastic scattering slope  $B_{pp}^{\text{el}}(s)$  as well as proton inclusive and diffractive SFs  $F_{2/p}(x, Q^2)$ ,  $F_{2/p}^{D(3)}(x, x_{\mathbb{P}}, Q^2)$ . The latter are given to leading order as

$$F_{2/p}(x, Q^2) = \sum_{I=q, \bar{q}} e_I^2 x f_{I/p}^{\text{scr}}(x, Q^2) + F_{2/p}^{(c)}(x, Q^2) \quad (37)$$

$$F_{2/p}^{D(3)}(x, x_{\mathbb{P}}, Q^2) = \sum_{I=q, \bar{q}} e_I^2 x f_{I/p}^{\text{diffr}}(x, x_{\mathbb{P}}, Q^2). \quad (38)$$

Here  $f_{I/p}^{\text{scr}}(x, Q^2) = \int d^2 b \tilde{f}_{I/p}^{\text{scr}}(x, b, Q^2)$ ,  $\tilde{f}_{I/p}^{\text{scr}}(x, b, Q^2)$  being obtained from (19) using  $\tilde{f}_{J/a}^{\text{scr}}(x, b, Q_0^2)$  defined in (33) as the initial conditions for sea quarks and gluons;  $f_{I/p}^{\text{diffr}}(x, x_{\mathbb{P}}, Q^2)$  are defined in (35-36). The charm quark contribution  $F_{2/p}^{(c)}(x, Q^2)$  has been calculated via the photon-gluon fusion process [22], using  $m_c = 1.3$  GeV for the charm quark mass, and neglected in the diffractive SF.

Concerning the parameter choice, we used the two-component picture with one “passive” component,  $\lambda_{p(2)} = 0$ , and with the standard value of the shower enhancement coefficient  $\lambda_{p(1)} = 1/C_{p(1)} = \sqrt{1.5}$ . It turned out that a reasonable agreement with data can be obtained even for a rather small virtuality cutoff  $Q_0^2 = 1$  GeV $^2$  for semi-hard processes; for the other parameters we obtained  $\alpha_P(0) = 1.15$ ,  $\alpha'_P(0) = 0.075$  GeV $^{-2}$ ,  $\gamma_p = 5.6$  GeV $^{-1}$ ,  $R_p^2 = 2.15$  GeV $^{-2}$ ,  $\gamma_{\mathbb{P}} = 0.5$  GeV $^{-1}$ ,  $G = 0.18$  GeV $^2$ ,  $\beta_g = 1$ ,  $w_{qg} = 0.22$ . The results are plotted in Figs. 10-12. For comparison we

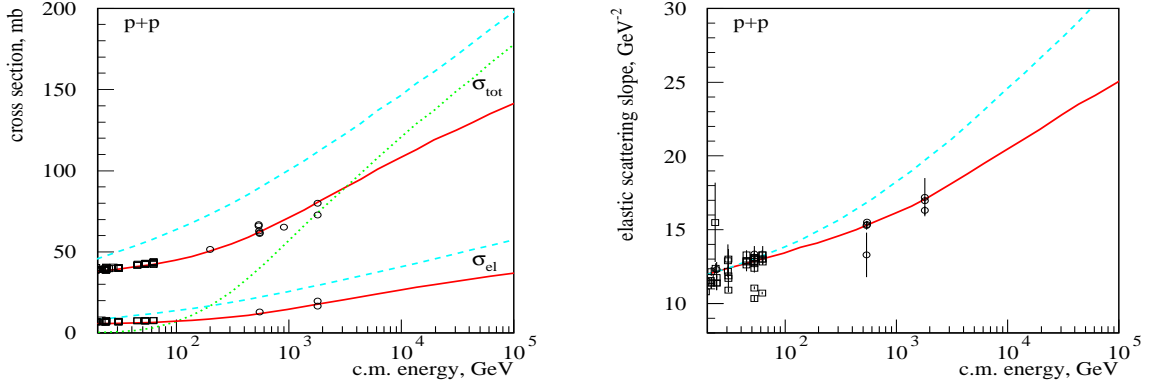


Figure 10: Total and elastic proton-proton cross sections (left) and elastic scattering slope (right) as calculated with and without enhanced diagram contributions - solid and dashed lines correspondingly. Dotted line corresponds to  $\sigma_{pp}^{\text{tot}}(s)$ , calculated using only the factorized contribution of semi-hard processes  $\chi_{pp}^{\text{sh(fact)}}(s, b)$ , as explained in the text. The compilation of data is from [23].

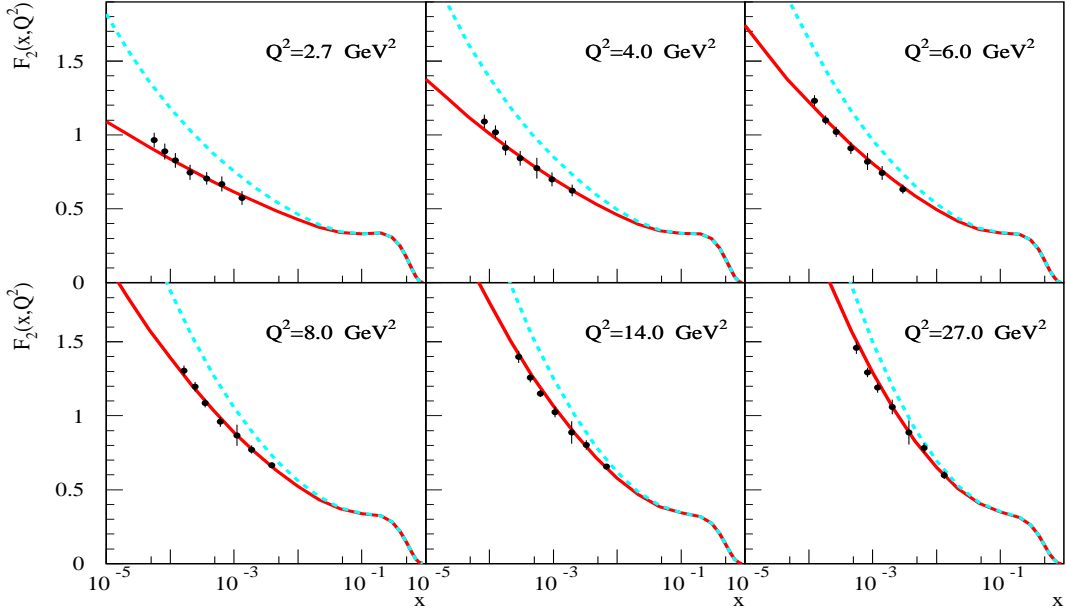


Figure 11: Proton SF  $F_{2/p}(x, Q^2)$  calculated with and without enhanced graph corrections - full and dashed lines correspondingly, compared to data of the ZEUS forward plug calorimeter [24].

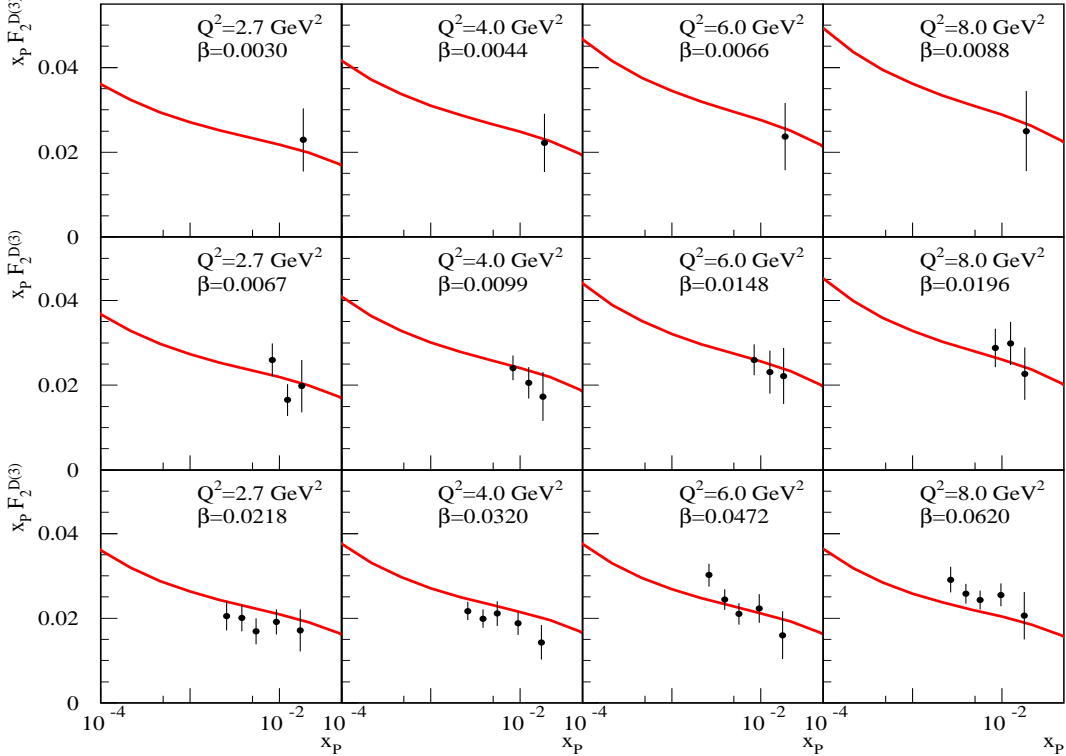


Figure 12: Proton diffractive SF  $x_p F_{2/p}^{D(3)}(x, x_p, Q^2)$ , compared to data of the ZEUS forward plug calorimeter [24].

show also  $\sigma_{pp}^{\text{tot}}$ ,  $\sigma_{pp}^{\text{el}}$ ,  $B_{pp}^{\text{el}}$ ,  $F_{2/p}$  as calculated without enhanced diagram contributions, i.e. using the eikonal  $\chi_{pp}(s, b)$  defined in (18) and the PDFs  $\tilde{f}_{I/p}(x, b, Q^2)$  given in (19), (16-17).

It is worth to note the differences with our previous treatment [12], which used only soft pomeron contributions and was based on the assumption of  $\pi$ -meson dominance of multi-pomeron vertices. Here, considering contributions of both soft and semi-hard processes and assuming a small slope of multi-pomeron vertices, we obtained an unusually small value for the soft pomeron slope. This is because the enhanced diagram contribution  $\chi_{ad(jk)}^{\text{enh}}(s, b)$ , defined in (29), is most significant in the region of comparatively small impact parameters, being characterized by a much smaller effective slope than the one of the soft pomeron. On the other hand, the obtained values of the pomeron intercept  $\alpha_P(0) = 1.15$  and of the triple-pomeron coupling  $r_{3P} = 4\pi G \gamma_P^3 \simeq 0.28 \text{ GeV}^{-1}$  are not too different from the ones in [12]: 1.18 and 0.18  $\text{GeV}^{-1}$  correspondingly.

It is important to stress that the full interaction eikonal (31), which includes the enhanced diagram contribution (29), can no longer be expressed in the usual factorized form (1), (18). In particular, non-linear screening corrections to the contribution of semi-hard processes can not be simply absorbed into the re-defined PDFs  $\tilde{f}_{I/a}^{\text{scr}}(x, b, Q^2)$ . Significant non-factorizable corrections come from graphs where at least one pomeron is exchanged in parallel to the hardest parton scattering process, with the simplest example given by the 1st diagram in the r.h.s. of Fig. 5. In fact, such contributions play an important role for reaching the consistency between total hadronic cross sections and structure functions. For the illustration, in Fig. 10 shown also the result for  $\sigma_{pp}^{\text{tot}}(s)$ , as calculated using only the factorized semi-hard contribution  $\chi_{pp}^{\text{sh(fact)}}(s, b)$ , i.e. using the eikonal (18) with  $\chi_{pp}^{\text{soft}}(s, b) \equiv 0$  and with the PDFs  $\tilde{f}_{I/p}(x, b, Q^2)$  being replaced by  $\tilde{f}_{I/p}^{\text{scr}}(x, b, Q^2)$ . It is easy to see that in such a case the cross section rises with energy much faster than obtained before with the full eikonal (31), even though the contribution of soft processes is neglected. At the same moment, due to the AGK cancellations [13], the above-mentioned non-factorizable graphs give negligible contribution to inclusive high- $p_t$  jet spectra. Single inclusive particle spectra are defined as usual by the diagrams of Fig. 13 [25]. In particular, inclusive jet spectra are thus given

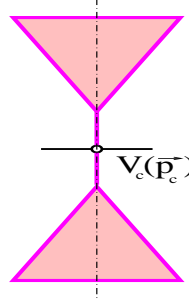


Figure 13: Diagrams contributing to single inclusive cross sections;  $V_c(\vec{p}_c)$  is the particle  $c$  emission vertex from a cut pomeron.

in the usual factorized form [26]: as the convolution of hadronic PDFs  $f_{I(J)/a(d)}^{\text{scr}}$  and the differential cross section  $\frac{d^3\sigma_{I,J,K}}{dp^3}$  for parton emission.

In conclusion, accounting for non-linear screening effects, one can obtain a consistent description of hadronic cross sections and of corresponding structure functions, using a fixed energy-independent virtuality cutoff for the contribution of semi-hard processes. An important feature of the proposed scheme is that the contribution of semi-hard processes to the interaction eikonal contains a significant non-factorizable part. On the other hand, by virtue of the AGK cancellations the corresponding diagrams do not contribute to inclusive parton jet spectra and the scheme preserves the QCD factorization picture.

## References

- [1] L. Gribov, E. Levin and M. Ryskin, Phys. Rep. **100**, 1 (1983).
- [2] A. Donnachie and P. Landshoff, Phys. Lett. B **332**, 433 (1994).
- [3] T. K. Gaisser and F. Halzen, Phys. Rev. Lett. **54**, 1754 (1985); L. Durand and P. Hong, *ibid.* **58**, 303 (1987); G. Pancheri and Y. N. Srivastava, Phys. Lett. B **182**, 199 (1986); T. K. Gaisser and T. Stanev, *ibid.* **219**, 375 (1989); X.-N. Wang, Phys. Rep. **280**, 287 (1997).
- [4] T. Sjostrand and M. van Zijl, Phys. Rev. D **36**, 2019 (1987); X.-N. Wang and M. Gyulassy, *ibid.* **44**, 3501 (1991); P. Aurenche *et al.*, *ibid.* **45**, 92 (1992); R. S. Fletcher *et al.*, *ibid.* **50**, 5710 (1994); I. Borozan and M. H. Seymour, JHEP **0209**, 015 (2002).
- [5] N. N. Kalmikov, S. S. Ostapchenko and A. I. Pavlov, Bull. Russ. Acad. Sci. Phys. **58**, 1966 (1994); Nucl. Phys. Proc. Suppl. B **52**, 17 (1997).
- [6] H. J. Drescher *et al.*, J. Phys. G: Nucl. Part. Phys. **25**, L91 (1999); S. Ostapchenko *et al.*, *ibid.* **28** (2002) 2597.
- [7] V. N. Gribov, Sov. Phys. JETP **26**, 414 (1968); *ibid.* **29**, 483 (1969).
- [8] M. Baker and K. A. Ter-Martirosian, Phys. Rep. **28**, 1 (1976); A. B. Kaidalov, *ibid.* **50**, 157 (1979).
- [9] A. H. Mueller and J. Qui, Nucl. Phys. B **268**, 427 (1986); A. H. Mueller, *ibid.* **335**, 115 (1990); L. McLerran and R. Venugopalan, Phys. Rev. D **49**, 2233 (1994); *ibid.* **49**, 3352 (1994); J. Jalilian-Marian *et al.*, *ibid.* **55**, 5414 (1997); Yu. V. Kovchegov and A. H. Mueller, Nucl. Phys. B **529**, 451 (1998).
- [10] F. W. Boop *et al.*, Phys. Rev. D **49**, 3236 (1994); K. J. Eskola *et al.*, Nucl. Phys. B **570**, 379 (2000); J. Dischler and T. Sjostrand, Eur. Phys. J. direct C **3**, 2 (2001); S.-Y. Li and X.-N. Wang, Phys. Lett. B **527**, 85 (2002).
- [11] O. V. Kancheli, JETP Lett. **18**, 274 (1973); J. L. Cardi, Nucl. Phys. B **75**, 413 (1974); A. Schwimmer, *ibid.* **94**, 445 (1975); A. Capella, J. Kaplan and J. Tran Thanh Van, *ibid.* **105**, 333 (1976); M. S. Dubovikov and K. A. Ter-Martirosyan, *ibid.* **124**, 163 (1977); V. A. Abramovskii, JETP Lett. **23**, 228 (1976); A. B. Kaidalov, L. A. Ponomarev and K. A. Ter-Martirosyan, Sov. J. Nucl. Phys. **44**, 468 (1986); S. Bondarenko *et al.*, Nucl. Phys. A **683**, 649 (2001).
- [12] S. Ostapchenko, Phys. Lett. B (to be published), hep-ph/0602139.
- [13] V. A. Abramovskii, V. N. Gribov and O. V. Kancheli, Sov. J. Nucl. Phys. **18**, 308 (1974).
- [14] M. Braun, Sov. J. Nucl. Phys. **52**, 164 (1990); V. A. Abramovskii and G. G. Leptoukh, *ibid.* **55**, 903 (1992); M. Hladik *et al.*, Phys. Rev. Lett. **86**, 3506 (2001).
- [15] M. L. Good and W. D. Walker, Phys. Rev. **120**, 1857 (1960).
- [16] A. B. Kaidalov and K. A. Ter-Martirosyan, Phys. Lett. B **117**, 247 (1982).
- [17] H. J. Drescher *et al.*, Phys. Rep. **350**, 93 (2001).
- [18] S. Bondarenko, E. Levin and C.-I. Tan, Nucl. Phys. A **732**, 73 (2004).
- [19] M. Gluck, E. Reya and A. Vogt, Z. Phys. C **67**, 433 (1995).

- [20] S. Ostapchenko, Nucl. Phys. Proc. Suppl. **151**, 143 (2006); in *proceedings of INFN Eloisatron Project 44th Workshop on QCD at Cosmic Energies*, Erice, Italy, 2004, hep-ph/0501093.
- [21] N. N. Nikolaev and B. G. Zakharov, Z. Phys. C **53**, 331 (1992); M. Genovese, N. N. Nikolaev and B. G. Zakharov, Sov. Phys. JETP **81**, 625 (1995); J. Bartels *et al.*, Eur. Phys. J. C **7**, 443 (1999).
- [22] M. Gluck, E. Reya and M. Stratmann, Nucl. Phys. B **422**, 37 (1994).
- [23] C. Caso *et al.*, Eur. Phys. J. C **3**, 1 (1998).
- [24] S. Chekanov *et al.*, ZEUS Collaboration, Nucl. Phys. B **713**, 3 (2005).
- [25] A. H. Mueller, Phys. Rep. **73**, 237 (1981).
- [26] J. F. Owens, Rev. Mod. Phys. **59**, 465 (1987).